Superconducting film with weak pinning centers: Incommensurate vortex lattices

G. R. Berdiyorov,[1] M. V. Milošević,[1,2] and F. M. Peeters[1,*]
[1]*Departement Fysica, Universiteit Antwerpen, Groenenborgerlaan 171, B-2020 Antwerpen, Belgium*
[2]*Department of Physics, University of Bath, Claverton Down, Bath BA2 7AY, United Kingdom*
(Received 20 June 2007; published 15 October 2007)

Vortex configurations in a superconducting film with a square array of small antidots are studied within the Ginzburg-Landau (GL) theory. We find that in addition to the conventional vortex structures at the matching fields, a variety of vortex states can be stabilized by decreasing the pinning strength of the antidots, including (i) the triangular vortex lattice where some vortices are pinned by the antidots and others are located between them, (ii) vortex line structures, and (iii) a lattice of vortex cluster structures around the empty pinning centers. Although these partially pinned vortex structures are obtained more frequently in field cooled experiments than the square pinned vortex lattice, they are not the lowest energy states, i.e., the ground state, contrary to the results from a London approach. This result can be understood as due to the presence of a broad local minimum in the GL free energy which keeps the vortices away from the pinning centers. Our results can also be related to recent experiments on macroscopic metallic particles that move in a plane in the presence of a weak electrostatic pinning potential.

DOI: 10.1103/PhysRevB.76.134508 PACS number(s): 74.20.De, 74.25.Dw, 74.78.Na, 74.25.Ha

I. INTRODUCTION

It is well known that the regular triangular vortex lattice has the lowest energy in defect-free superconductors,[1] which is due to the isotropic repulsive interaction between the vortices. If a square lattice of pinning centers is present, it will impose its own symmetry on the vortex structure. Direct imaging experiments[2] and theoretical calculations[3,4] have shown that in superconductors with a square pinning array, the vortices form highly ordered configurations when the number of vortices is a multiple or rational multiple of the number of pinning sites. These commensurability effects between the pinning centers and the vortex lattice are reflected in an enhancement of the critical current, resulting from the collective locking of vortices to the pinning sites.[5–8]

If the vortex-pinning strength in a periodic square array is reduced, the vortex-vortex repulsion starts to dominate over the pinning force and the triangular lattice is recovered. Calculations within the London theory,[9] where vortices are considered as pointlike particles, show that depending on the strength and length scale of the pinning potential, the triangular vortex lattice where some vortices are pinned by the pinning sites and others are located between them can become the ground state. A phase diagram for the transition between these two vortex states was given in Ref. 9, which strongly depends on the periodic pinning potential parameters. These kinds of partially pinned (PP) phases have recently been demonstrated experimentally for macroscopic Wigner crystals in square pinning arrays.[10] In this experiment, the transition between the square pinned and the PP states occurs sharply with decreasing pinning strength. We would like to mention that the effect of weak pinning is very important for the vortex matter in superconductors, especially in high-T_c superconductors. In the latter case, the vortex system is strongly affected by the finite pinning force (from, e.g., crystal structure anisotropy, thermal fluctuations), leading to the distortion of the triangular vortex lattice, i.e., the Bragg glass phase (see as an example Ref. 11 and references therein).

In this work, we study different vortex configurations in a superconducting film with a square array of antidots within the Ginzburg-Landau theory. With lowering the pinning force (i.e., small radius of antidots), deformed triangular vortex structures are obtained, which results from the competition between the symmetry imposed by the pinning array and the symmetry of the unpinned vortex lattice. However, these partially pinned vortex states do not appear as a ground state, contrary to the calculations within the London limit and experiments on macroscopic charged particles. We find that the reason for the observation of the PP states in the experiment is the presence of a broad energy minimum in configuration space where the system becomes favorably trapped in a metastable state. In this state, vortices are depinned and located at the interstitial sites.

II. THEORETICAL FORMALISM

We consider a superconducting film (of thickness d) with a square array of circular holes (of radius R and period W) in the presence of a perpendicular uniform magnetic field H (see Fig. 1). For the given system, we solved two nonlinear Ginzburg-Landau (GL) equations, which can be written in dimensionless units in the following form:

$$(-i\nabla - \mathbf{A})^2\Psi = \Psi(1 - |\Psi|^2), \tag{1}$$

$$-\Delta\mathbf{A} = \frac{d\xi}{\lambda^2}\delta(z)\mathbf{j}, \tag{2}$$

where

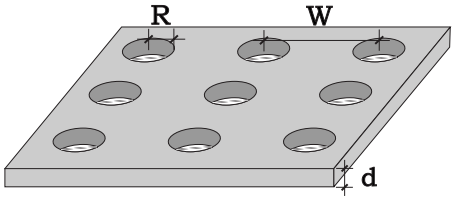

FIG. 1. Schematic view of the sample: a superconducting film (thickness d) with a square array (period W) of circular antidots (radius R).

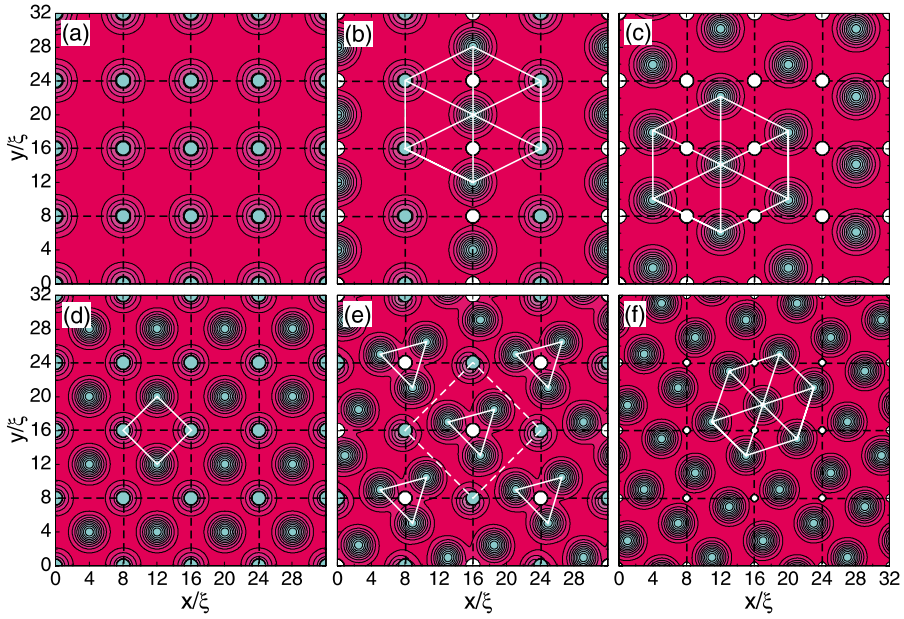

FIG. 2. (Color online) Contour plots of the Cooper-pair density in the superconducting film of thickness $d=0.1\xi$ with antidots of radius [(a)–(e)] $R=0.8\xi$ and (f) $R=0.4\xi$ and period $W=8\xi$ at the [(a)–(c)] first $H=H_1$ and [(d)–(f)] second $H=H_2$ matching fields for [(a) and (d)] the totally pinned and [(b), (c), (d), and (f)] the partially pinned states. Pink (dark gray) regions correspond to high density and cyan (light gray) denotes low density. Dashed black lines show the antidot lattice, white lines show the vortex lattice, and white dots are antidots without a vortex.

$$\mathbf{j} = \frac{1}{2i}(\Psi^* \nabla \Psi - \Psi \nabla \Psi^*) - |\Psi|^2 \mathbf{A} \tag{3}$$

is the density of the superconducting current in the plane $[\rho=(x,y)]$. Here, all distances are expressed in units of ξ, the vector potential in $\Phi_0/2\pi\xi$, and the order parameter in $\Psi_0 = \sqrt{-\alpha/\beta}$ with α and β the GL coefficients. Equations (1) and (2) are solved using the iterative procedure from Ref. 12 in combination with the link-variable approach[13] (see Ref. 4 for more details). The magnitude of the applied magnetic field $H=n\Phi_0/S=H_n$ is determined by the number n of quantum fluxes $\Phi_0=hc/2e=2.07\times10^{-7}$ G cm^2 piercing through the simulation region area S. In this work, we focus on the case of $H/H_1 \leqslant 3$, where H_1 is the field at which there is one vortex per antidot, i.e., the first matching field. Simulations are done for a 2×2 unit cell. We have also conducted simulations for larger unit cells and have found the same features as found for the 2×2 system. The following periodic boundary conditions are used for $\mathbf{A}$ and Ψ around the square simulation region:[14]

$$\mathbf{A}(\mathbf{r}+\mathbf{b}_i) = \mathbf{A}(\mathbf{r}) + \nabla \eta_i(\mathbf{r}), \tag{4}$$

$$\Psi(\mathbf{r}+\mathbf{b}_i) = \Psi \exp[2\pi i \eta_i(\mathbf{r})/\Phi_0], \tag{5}$$

where $\mathbf{b}_i$ $(i=x,y)$ is the lattice vector and η_i is the gauge potential. At the same time, the condition $j_\perp=0$ was used at the boundaries of the antidots. The dimensionless Gibbs free energy (in units of $F_0=H_c^2/4\pi$) is calculated as

$$F = V^{-1} \int [-|\Psi|^4 + 2(\mathbf{A}-\mathbf{A}_0)\mathbf{j}]dV, \tag{6}$$

where integration is performed over the primitive cell volume V, and $\mathbf{A}_0$ is the vector potential of the external applied uniform magnetic field. Temperature is included in the calculations through the temperature dependence of the coherence length $\xi(T)=\xi(0)/\sqrt{|1-T/T_{c0}|}$ and the penetration depth $\lambda(T)=\lambda(0)/\sqrt{|1-T/T_{c0}|}$, where T_{c0} is the critical temperature at zero applied field.

III. STABLE VORTEX CONFIGURATIONS

Figures 2(a)–2(c) show the three different vortex configurations at the first matching field found from a numerical solution of the coupled GL equations. The first state is the one with all vortices pinned by the holes [totally pinned (TP) state] [Fig. 2(a)], i.e., the vortex lattice has the same highly symmetric structure as the pinning lattice. In Fig. 2(b), half of the vortices are pinned by the holes and the others are depinned and located between the antidots (i.e., the PP state). The alternating rows of pinned and unpinned vortices restore the triangular symmetry of the vortex lattice and correspond to the vortex state found in the experiment[10] on metallic particles and predicted by the London theory.[9] A third possible vortex state is the one where all the vortices are depinned which form again a triangular lattice [Fig. 2(c)].

At the second matching field in the TP state, all pinning centers are occupied and the remaining vortices are located at the interstitial region. The overall vortex lattice is a square but rotated over 45° with respect to the pinning array [Fig. 2(d)]. The PP state [Fig. 2(e)] is the one with one hole occupied by the vortices and the next one is empty. Three unpinned vortices form clusters around the empty holes and all

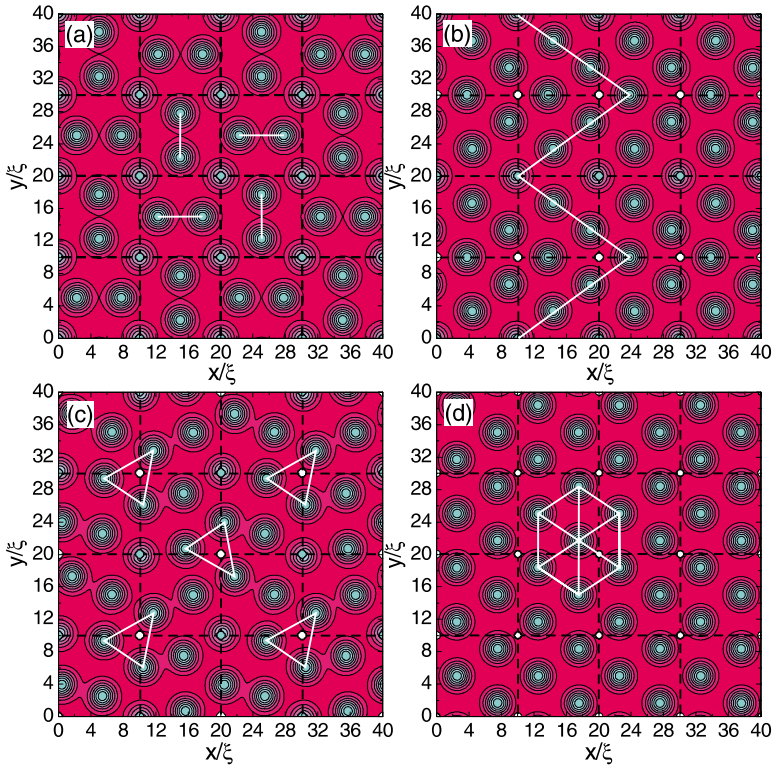

FIG. 3. (Color online) (a) Totally pinned and [(b)–(d)] partially pinned states at the third matching field $H=H_3$. The period is $W=10\xi$, the radius is $R=0.5\xi$, and the thickness is $d=0.1\xi$.

the clusters are oriented in the same direction. The orientation of the vortex clusters is different from the one obtained in the experiment,[10] where the clusters are oriented along the axis of the pinning array. However, vortex cluster orientation changes gradually to the experimentally obtained one with further increasing the distance between the antidots. These clusters, or trimers, shown here are not perfect equilateral triangles because of the influence of the pinned vortices. For small radius of antidots, all the vortices are depinned and arrange themselves into a deformed triangular lattice [Fig. 2(f)].

Four possible vortex states at $H=H_3$ are shown in Fig. 3. For small radius of the antidots, we obtain a slightly distorted triangular lattice with all the vortices located at the interstitial sites [Fig. 3(d)]. In the PP state [Fig. 3(c)], half of the antidots are occupied by vortices and the interstitial vortices tend to cluster around the empty antidots as in the case of the second matching field [see Fig. 2(e)]. However, large vortex clusters are not present, which could be expected from the results for the second matching field. Another PP state at $H=H_3$ is shown in Fig. 3(b), which consists of alternating rows of occupied and unoccupied holes with a zigzag structure of interstitial vortices. The TP state consists of one pinned and two interstitial vortices which alternate in position from one interstitial site to another [Fig. 3(a)]. We have also conducted simulations for $H>H_3$ and observed the same general features of the vortex states as outlined above, but with a larger number of possible vortex configurations.

IV. STABILITY ANALYSIS OF THE VORTEX STATES

The existence of several vortex configurations for a given magnetic field is an indication of the occurrence of possible stable and metastable states. Although the PP states are observed more frequently than the TP states in the experiments with charged particles,[10] it was concluded that these states are degenerate, whereas in calculations within the London theory, the PP states were found to be a ground state. In what follows, we perform a detailed analysis of these vortex states including material properties (through the GL parameter κ) and temperature.

Usually, in experiments on vortex structures (or structures of any interacting particles), so called "field cooled" measurements are carried out and the most frequently observed patterns are referred to as stable configurations and less frequent states are considered as metastable configurations. Recent Bitter decoration experiments[15] on the vortex structure in mesoscopic superconducting samples have shown that for the same magnetic field and the same sample parameters, different vortex configurations could be found with the same number of vortices. After a statistical analysis, the most often found vortex configuration was assumed to be the ground state, while the others were considered to be metastable states. Furthermore, a small number of the theoretically predicted vortex states[16] were never seen in the experiment and some of them were found in few cases and, therefore, were considered as metastable states. A recent theoretical analysis[17] showed that the vortex configurations are not universal and depend on the size and thickness of the superconducting disk.

We conducted a field cooled experiment, which gives us the possibility to study the statistics of the TP and the PP states. We started from a random initial vortex distribution for a given field and sample parameters and followed the evolution of the system into one of the (meta)stable states. The results are shown in Fig. 4(a) for $H=H_1$. It is seen from

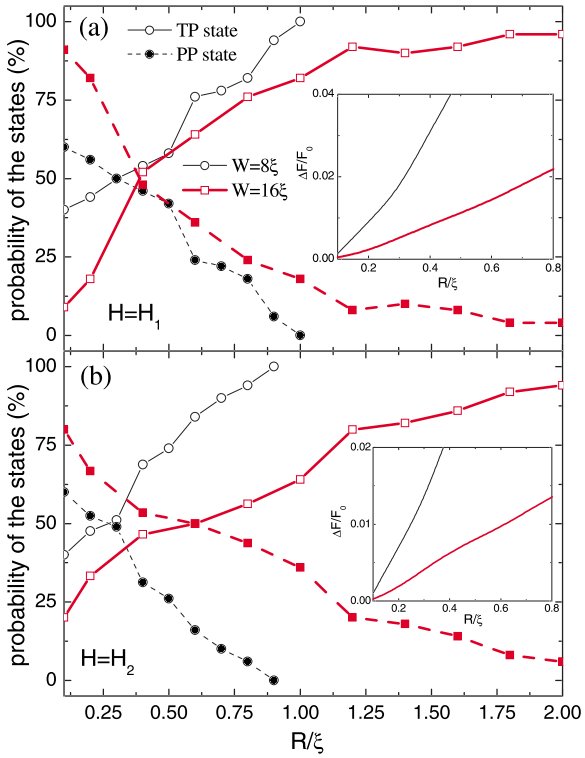

FIG. 4. (Color online) Probability to find the totally pinned (TP) (solid curves, open symbols) and partially pinned (PP) (dashed curves, filled symbols) vortex states as a function of the hole radius R for two different periods W at (a) $H=H_1$ and (b) $H=H_2$. The film thickness is $d=0.1\xi$ and the effective GL parameter is equal to $\kappa^*=\kappa^2\xi/d=\infty$. The insets show the energy difference ΔF between the TP and the PP vortex states as a function of the radius R.

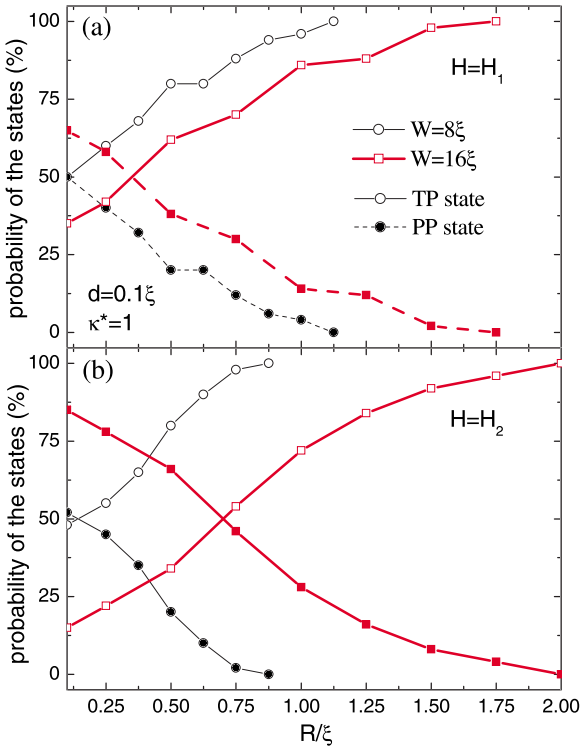

FIG. 5. (Color online) The same as in Fig. 4 but now for the effective GL parameter $\kappa^*=1$.

this figure that the PP state is obtained more frequently than the TP state for small pinning force (i.e., small hole radius R). However, there is no sharp transition to the 100% PP state. Increasing the hole radius leads to a decrease of the probability to obtain the PP state. Larger period W requires larger radius R in order to have 100% TP state. In spite of the fact that the probability to obtain the PP state from a random distribution of vortices is much higher than the probability to obtain the TP state, the PP state turns out to have always a higher energy than the TP state for the given field. This is shown in the inset of Fig. 4(a) by the free energy difference between the PP and TP states, $\Delta F=F_{PP}-F_{TP}$. It is seen from this figure that ΔF becomes smaller with decreasing the radius R, as well as with increasing interhole distance W for a fixed R, but vortices always prefer to form a square symmetric state for very small radius. The same behavior of the PP and TP states is found for the second matching field [see Fig. 4(b)]. A small difference is that the probability of the PP state is smaller for small period of the pinning lattice W and larger for larger W, compared to the results for $H=H_1$. The latter is related to different density of the flux lines.

Let us now see how the vortex-vortex interaction force affects our results. It is well known that the effective interaction between the vortices is determined by the GL parameter $\kappa=\lambda/\xi$ (in thin superconductors, $\kappa^*=\kappa^2\xi/d$). We performed the same statistical analysis as shown in Fig. 4 for smaller κ values. As an example, we plot in Fig. 5, for the GL parameter $\kappa^*=1$, the probability to find the PP (dashed curves) and TP (solid curves) states as a function of the radius of the antidots for different values of the interhole distance for (a) $H=H_1$ and (b) $H=H_2$. It is seen from this figure that the probability to find the PP state decreases considerably with decreasing κ^* to $\kappa^*=1$ compared to larger κ^* case (Fig. 4) for both applied field values. This is due to the dominance of the vortex-pinning site interaction over the decreased vortex-vortex interaction.

So far, we presented results at fixed temperature. In what follows, we include temperature in our numerical analysis through the temperature dependence of the coherence length ξ (see Sec. II). We now consider a superconducting film with thickness $d=20$ nm, interhole distance $W=1$ μm, and antidot radii $R=20$ nm and $R=50$ nm. We choose the coherence length $\xi(0)=40$ nm and the penetration depth $\lambda(0)=42$ nm (the effective GL parameter is $\kappa^*=\lambda^2/\xi d=2.21$), which are typical values for Pb films. Figure 6 shows the temperature dependence of the probability to realize the TP (solid curves) and PP (dashed curves) states at the second matching field when starting from a random distribution of vortices. It is seen from this figure that the evolution of the states weakly depends on temperature, in spite of the fact that temperature effectively changes the pinning force of the antidots. This result indicates that a larger energy barrier is separating different vortex states. The effect of temperature becomes important close to T_c, where the vortex lattice undergoes a transition from the PP state to 100% TP state for both radii of the antidots. Note that for $R=25$ nm, the PP state dominates over the TP state, while for $R=50$ nm, the opposite is found.

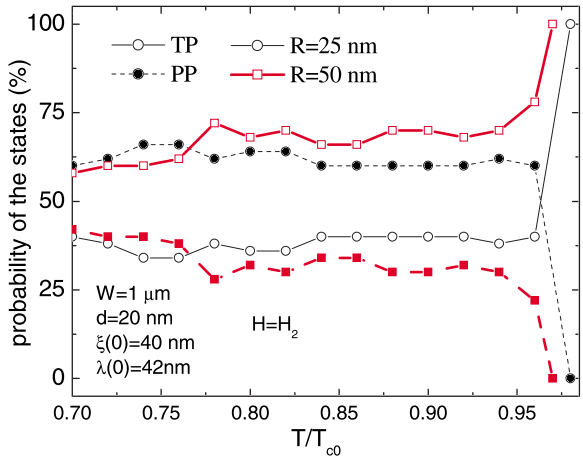

FIG. 6. (Color online) The statistics of the TP (solid curves, open symbols) and PP (dashed curves, filled symbols) states as a function of temperature. Parameters of the sample are given in the figure.

V. DISCUSSION

The unexpected result that the most probable vortex state is not necessarily the ground state can be elucidated by the following simple consideration. From the fact that the PP vortex configurations are observed more frequently than the TP vortex state for small pinning strengths, one can conclude that the PP state has a larger interval of stability. This can be checked by calculating the free energy of a superconducting disk with a hole (we considered a large disk in order to reduce the effect of the boundary) as a function of the position of the vortices inside the disk. We followed the approach given in Ref. 18 to calculate the free energy of the system for the applied magnetic field $H=2n\Phi_0/S$, where n is the number of vortices and S is the surface area of the sample.

When there is only one vortex in the disk, it interacts attractively with the hole [Fig. 7(a)] and the system has the lowest energy when the vortex is inside the hole. The presence of two or more vortices in the sample changes this attractive interaction [see Fig. 7(b), where we fixed one vortex and the other two were free to move in order to minimize the energy]. The pinning force to the hole is now compensated by the repulsive interaction between the vortices and the free energy exhibits a very broad minimum for a nonzero separation distance, depending on the size of the hole. Because of this broad minimum in the energy, vortices are easily pinned in the interstitials, increasing the probability to obtain the PP state. However, if one of the vortices comes close to the hole and occupies it (or the vortex is initially in the hole), the free energy of the system becomes even lower. However, this minimum in the free energy is very narrow (see the black curve in the figure). Therefore, in order to find the ground state vortex configuration, we have to put one vortex exactly in the hole, otherwise the system will most probably move to the broader energy minimum, forming a trimer around the hole. In the latter case, vortices are located

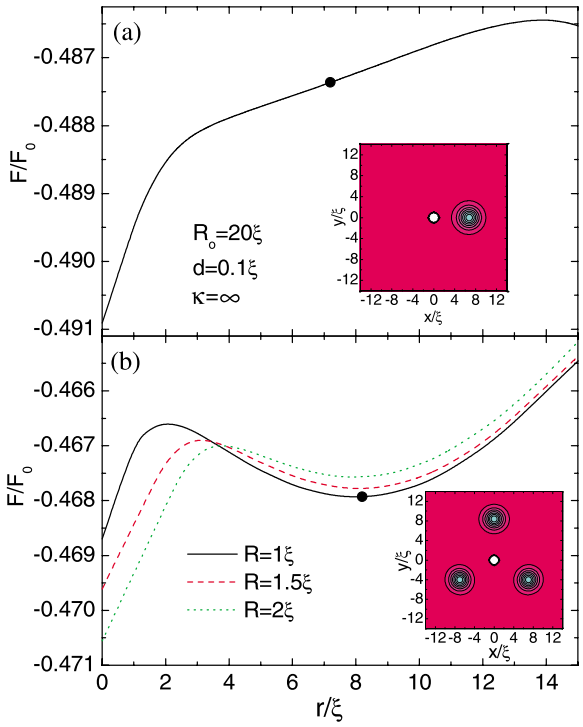

FIG. 7. (Color online) The free energy of an individual disk of radius $R_o=20\xi$ and thickness $d=0.1\xi$ as a function of the radial position of the vortex r from the disk center for different values of the hole radius R and for different number of vortices n in the sample: (a) $n=1$ and (b) $n=3$. The insets show the Cooper-pair density plots corresponding to the circles on the free energy curve.

equidistantly from the hole [see also Fig. 2(e)]. If we now increase the radius of the hole, the minimum in the free energy corresponding to all vortices sitting in the superconducting region moves up in energy. At the same time, this minimum becomes less pronounced, decreasing the probability to realize the PP states.

VI. CONCLUSIONS

We studied the vortex lattice structures in a superconducting thin film with a square array of weak pinning antidots within the GL theory. When the pinning force of the antidots is small, i.e., small radius of the antidots, the triangular vortex lattice becomes energetically favorable. Depending on the applied field, all the vortices can be located between the antidots, or some of them are pinned by the antidots and some of them are located between the pinning centers. In some cases, vortices do not form a simple lattice but arrange themselves in clusters around the empty pinning centers having a specific orientation.

Although these partially pinned vortex structures are obtained more frequently in field cooled experiments than the square pinned vortex lattice, they are not the ground state vortex configuration, contrary to the results from a London approach.[9] The reason for the larger probability to realize the partially pinned states is the broader energy minimum originating from the repulsive interaction between the vortices.

The statistics to obtain the PP and TP states weakly depend on the temperature, whereas the GL parameter κ, which determines the efficiency of the vortex-vortex interaction, strongly influences the obtained results. Our theoretical results imply that experimentally the most probably found vortex configuration is not necessarily the lowest energy vortex state.

ACKNOWLEDGMENTS

This work was supported by the Flemish Science Foundation (FWO-Vl), the Belgian Science Policy (IAP), and the ESF-AQDJJ network. M.V.M acknowledges support from EU Marie-Curie Intra-European Program and G.R.B acknowledges support from FWO-Vlaanderen.

*francois.peeters@ua.ac.be

[1] W. H. Kleiner, L. M. Roth, and S. H. Autler, Phys. Rev. **133**, A1226 (1964).
[2] K. Harada, O. Kamimura, H. Kasai, T. Matsuda, A. Tonomura, and V. V. Moshchalkov, Science **274**, 1167 (1996).
[3] C. Reichhardt, C. J. Olson, and Franco Nori, Phys. Rev. B **57**, 7937 (1998); C. Reichhardt and N. Gronbech-Jensen, Phys. Rev. Lett. **85**, 2372 (2000); C. Reichhardt, G. T. Zimanyi, and N. Gronbech-Jensen, Phys. Rev. B **64**, 014501 (2001); C. Reichhardt and N. Gronbech-Jensen, *ibid.* **63**, 054510 (2001).
[4] G. R. Berdiyorov, M. V. Milošević, and F. M. Peeters, Phys. Rev. Lett. **96**, 207001 (2006).
[5] V. V. Moshchalkov, M. Baert, V. V. Metlushko, E. Rosseel, M. J. Van Bael, K. Temst, R. Jonckheere, and Y. Bruynseraede, Phys. Rev. B **54**, 7385 (1996).
[6] V. V. Moshchalkov, M. Baert, V. V. Metlushko, E. Rosseel, M. J. Van Bael, K. Temst, Y. Bruynseraede, and R. Jonckheere, Phys. Rev. B **57**, 3615 (1998).
[7] L. Van Look, B. Y. Zhu, R. Jonckheere, B. R. Zhao, Z. X. Zhao, and V. V. Moshchalkov, Phys. Rev. B **66**, 214511 (2002).
[8] V. Metlushko, U. Welp, G. W. Crabtree, R. Osgood, S. D. Bader, L. E. DeLong, Zhao Zhang, S. R. J. Brueck, B. Ilic, K. Chung, and P. J. Hesketh, Phys. Rev. B **60**, R12585 (1999).
[9] W. V. Pogosov, A. L. Rakhmanov, and V. V. Moshchalkov, Phys. Rev. B **67**, 014532 (2003).
[10] G. Coupier, M. Saint Jean, and C. Guthmann, Phys. Rev. B **75**, 224103 (2007).
[11] K. Shibata, T. Nishizaki, M. Maki, and N. Kobayashi, Phys. Rev. B **72**, 014525 (2005).
[12] V. A. Schweigert, F. M. Peeters, and P. S. Deo, Phys. Rev. Lett. **81**, 2783 (1998).
[13] R. Kato, Y. Enomoto, and S. Maekawa, Phys. Rev. B **47**, 8016 (1993).
[14] M. M. Doria, J. E. Gubernatis, and D. Rainer, Phys. Rev. B **39**, 9573 (1989).
[15] I. V. Grigorieva, W. Escoffier, J. Richardson, L. Y. Vinnikov, S. Dubonos, and V. Oboznov, Phys. Rev. Lett. **96**, 077005 (2006).
[16] V. M. Bedanov and F. M. Peeters, Phys. Rev. B **49**, 2667 (1994); B. J. Baelus, L. R. E. Cabral, and F. M. Peeters, *ibid.* **69**, 064506 (2004).
[17] V. R. Misko, B. Xu, and F. M. Peeters, Phys. Rev. B **76**, 024516 (2007).
[18] G. R. Berdiyorov, L. R. E. Cabral, and F. M. Peeters, J. Math. Phys. **46**, 095105 (2005).